JOURNAL OF AGRICULTURAL AND FOOD CHEMISTRY

Bioactive Constituents, Metabolites, and Functions

Novel Biomedical Functions of Surfactin A from Bacillus subtilis in Wound Healing Promotion and Scar Inhibition

Lu Yan, Guanwen Liu, Bin Zhao, Bing Pang, Wanqin Wu, Chongyang Ai, Xixi Zhao, Xinglong Wang, Chunmei Jiang, Dongyan Shao, Qianlong Liu, Meixuan Li, Lei Wang, and Junling Shi

J. Agric. Food Chem., **Just Accepted Manuscript** • DOI: 10.1021/acs.jafc.0c01658 • Publication Date (Web): 15 May 2020

is published by the American Chemical Society. 1155 Sixteenth Street N.W., Washington, DC 20036

Novel Biomedical Functions of Surfactin A from *Bacillus subtilis* in Wound Healing Promotion and Scar Inhibition

Lu Yan,[†] Guanwen Liu,[†] Bin Zhao,[†] Bing Pang,[†] Wanqin Wu,[†] Chongyang Ai,[†] Xixi Zhao,[†] Xinglong Wang,[‡] Chunmei Jiang,[†] Dongyan Shao,[†] Qianlong Liu,[†] Meixuan Li,[†] Lei Wang,[†] and Junling Shi *[,†]

[†]Key Laboratory for Space Bioscience and Biotechnology, School of Life Sciences, Northwestern Polytechnical University, Xi'an, Shaanxi Province 710072, China

[‡]College of Veterinary Medicine, Northwest A&F University, Yangling, Shaanxi Province 712100, China

*Corresponding Author: E-mail: sjlshi2004@nwpu.edu.cn; Tel: +86-029-88460543; Fax: +86-029-88460543.

ABSTRACT: Surfactin produced by *Bacillus subtilis* is a powerful biosurfactant in food, cosmetics and pesticide industries. However, its suitability in wound healing applications is uncertain. In this article, we identified the effects of surfactin A from *B. subtilis* on wound healing, angiogenesis, cell migration, inflammatory response, and scar formation. The results indicated that 80.65±2.03 % of surfactin A-treated wounds were closed, whereas 44.30±4.26 % of the vehicle-treated wound areas remained open at day 7 ($P < 0.05$). In mechanisms, it up-regulated the expression of hypoxia inducible factor-1α (HIF-1α) and vascular endothelial growth factor (VEGF), accelerated keratinocyte migration through mitogen-activated protein kinase (MAPK) and nuclear factor-κB (NF-κB) signaling pathways, and regulated the secretion of pro-inflammatory cytokines and macrophage phenotypic switch. More attractive, surfactin A showed a seductive capability to inhibit scar tissue formation by affecting the expression of α-smooth muscle actin (α-SMA) and transforming growth factor (TGF-β). Overall, the study revealed a new function and potential of surfactin A as an affordable and efficient wound healing drug.

KEY WORDS: *Bacillus subtilis, surfactin A, wound healing, cell migration, scar inhibition.*

26 ■ **INTRODUCTION**

27 Surfactin is an amphipathic cyclic lipopeptide that is constituted by a heptapeptide sequence
28 linked to a ß-hydroxy fatty acid with 13-15 carbon atoms to form a close cyclic lactone ring
29 structure.[1] It is generally produced by various strains of *Bacillus subtili*s that has been widely
30 accepted as a biotic pesticide, bacterial fertilizer, and soil remediation agent in agriculture fields,
31 an attractive antimicrobial agent in food fields, and an effective probiotic in livestock feed.[2,3] Due
32 to its special molecular structure, surfactin has been recognized as one of the most powerful
33 biosurfactants and applied in foam creation and stabilization in food processing, solubilization of
34 agrochemicals, and bioremediation of water-insoluble pollutants.[4,5] Surfactin was also found to
35 exhibit strong anti-adhesion and antibiofilm ability against various food-borne pathogens on
36 material surfaces.[6] In previous studies, surfactin has also been reported to have attractive bioactive
37 functions in biopharmaceutical applications because of their anti-inflammatory, anti-microbial,
38 anti-cancer and anti-viral activities.[7] However, the capability of surfactin on wound healing is
39 barely tapped up to now. Development of surfactin's new functions will be important to expand its
40 applications in the food and agriculture fields.

41 Skin is an animal's first barrier to defend against the damage from environments.[8,9] Once this
42 barrier is broken, the wound healing process is triggered at the wound site to repair skin integrity
43 and restore its normal function.[10] Wound healing is an orchestrated and dynamic interplay
44 involving three overlapping phases: inflammation, cell proliferation, and extracellular matrix
45 remodeling.[11] In some cases, such as diabetes, smoking, aging, starvation and surgery, healing in
46 these wounds are delayed, which lead to enormous illness and even death.[12] Chronic wounds also
47 threaten the health of animals such as wound dehiscence in horses or cautery disbudding wounds
48 in dairy calves, and the nursing of such wounds is of great value to the development of livestock

in the agriculture.[13,14] Although various growth factors and peptides in animal skin were found to be effective for wound healing, high cost of extraction or synthesis operation bring serious economic burden to their application in disease treatment. [15,16] Therefore, it makes sense to develop natural products that are both cheap and effective for wound therapy.

Microorganism is one of the most promising resources to produce functional materials due to their wide spread, easy manipulations, and diverse metabolites.[17,18] In recent years, *B. subtilis* is gaining attention as a microbial factory because of its superior capacity to efficiently secret bioactive cyclic lipopeptides.[19] The antimicrobial and anti-adhesion activities of surfactin have been reported in wound dressing application.[20,21] Antioxidant activity of lipopeptide mixtures has also been implicated in promoting skin wound healing in a rat model.[22] However, there is no clear research on whether lipopeptide components can influence the biological process of wound healing. If surfactin can promote wound healing, the mechanism of its action is not clear.

As part of researches to exploit novel function of *B. subtilis* surfactin, we sought to understand the impacts of surfactin A from *B. subtilis* on different stages of wound healing in mice model. We focused on the effects of surfactin A from *B. subtilis* on angiogenesis, cell migration, inflammatory response and scar tissue *in vivo* and *in vitro*. In addition, the signaling pathways and molecules involved in the wound healing process were also investigated.

■ MATERIALS AND METHODS

Chemicals. Surfactin (MW: 1036.34 Da, purity ≥ 98%) was purchased from FUJIFILM Wako Pure Chemical Corporation (Osaka, Japan) and used as the standard surfactin A. Epidermal growth factor (EGF, purity ≥ 97%) and lipopolysaccharides (LPS) were purchased from Sigma-Aldrich (Shanghai, China). 3-(4,5-dimethylthiazol-2-yl)-2,5-diphenyl-2H-tetrazolium bromide

71 (MTT) and DMSO were purchased from Solarbio Science & Technology Co., Ltd. (Beijing,
72 China). Enzyme-linked immunosorbent assay (ELISA) was obtained from Elabscience
73 Biotechnology Co., Ltd (Wuhan, China). Acetonitrile (ACN), trifluoroacetic acid (TFA),
74 paraformaldehyde, formic acid, sodium sulfide, ethanol, paraffin wax, and hematoxylin and eosin
75 (H&E) were provided by Sinopharm Chemical Reagent Co., Ltd (Shaanxi, China).

76 **Preparation of *B. subtilis* Lipopeptides.** Crude lipopeptides were prepared from the culture
77 of *B. subtilis* strain CCTCC M207209 (GenBank: MT373810; **Figure S1**) according to the
78 previously developed method.[23] Then different fractions of crude lipopeptides were separated
79 using a chromatographic system AKTA purifier 10 (Amersham Brosciences, USA) equipped with
80 a C18 reversed phase chromatography (RPC) column (Resource^{TM} RPC 3mL, GE Healthcare,
81 Sweden). Elution was carried out with a linear-gradient of 0-100 % ACN containing 0.01% (v/v)
82 TFA in 0.01% TFA/water solvent system. Each eluted fraction was monitored at 280 nm. Different
83 fractions were separately collected according to the UV-absorbing peaks, analyzed in their
84 capability to promote wound healing process. Further purification was performed using high
85 performance liquid chromatography (HPLC) and the major component (Comp-2) was subjected
86 to analysis mass spectrometry to determine its precise structure. [23]

87 **Identification of the Active Lipopeptide Fraction by MALDI-TOF-MS.** The Comp-2 with
88 the ability to promote wound healing was analyzed using an UPLC I-Class system coupled to a
89 Vion IMS QTof mass spectrometer (Waters Corporation, Milford, MA, USA) as described with
90 minor modifications.[24] The analysis was performed at 35 °C using an Acquity UPLC C18 BEH
91 (50 mm × 2.1 mm, 1.7 μm) column (Waters Corporation, Milford, MA, USA). The mobile phase
92 consisted of 0.1% formic acid in water (A) and ACN (B). The flow rate was maintained at 0.4
93 mL/min with elution gradient of 8 min (5-70 %, v/v B for 3 min; 70 %, v/v B for 1 min; 70-100

94 %, v/v B for 1 min; 100 %, v/v B for 1 min; 100-5 %, v/v B for 1 min). Sample injection volume
95 was 2 μL and the mass spectrometer was recorded on positive ion mode at a mass range of 100-
96 2000 m/z. Molecular ions detected were further characterized by MS/MS measurement. Mass
97 range for fragmentation was 50-1500 m/z and the high collision energy was ramped from 20 to
98 45 eV. Data were deconvoluted using MassLynx 4.1 software (Waters Co., Milford, USA).

99 **Verification of The Active Lipopeptide Fraction.** According to the results, surfactin A was
100 identified as the most active lipopeptide fraction produced by *B. subtilis* to promote wound healing
101 process (**Figure 2**). In order to verify the wound healing activity of surfactin A and reveal the
102 mechanisms, purified surfactin A was used in the following studies. Wound healing capability
103 experiments were carried out in mice and the mechanism analysis experiments were carried out in
104 cells that might be involved in the wound healing process. Mice macrophage cells (Raw 264.7),
105 immortalized human keratinocytes (HaCaT), human dermal fibroblasts (HDF), and human
106 umbilical vein endothelial cells (HUVEC) cells were obtained from the American Type Culture
107 Collection (ATCC, Manassas, VA, USA) and used for the mechanism analysis. All types of cells
108 were cultured at 37 °C and 5% CO_2 in relevant medium (Hyclone, Logan, USA) supplemented
109 with 10% FBS (TransSerum TM HQ, USA) and 1% (v/v) antibiotic-antimycotic.

110 **Construct of Full-Thickness Excisional Wounds Model in Mice.** All protocols used in the
111 study were approval by the Animal Care and Experimental Committee of Northwestern
112 Polytechnical University School of Life Science. Male Kunming murine (age 6-8 week, weighing
113 ≈ 25 g) were selected and observed for a week before operation. All murine were anesthetized
114 using 1.5% pentobarbital sodium with a dose of 70 mg/kg body weight. For asceptic surger, dorsal
115 hairs were removed via 7% sodium sulfide, then disinfected using 75% ethanol. Circular skin
116 wounds were made with a 7-mm-diameter biopsy punch on the back of each mouse and the skin

117 was removed.[25] After wounding, the murine were caged individually and the wounds were not
118 covered. 100 μg/mL surfactin A or 100 μg/mL EGF dissolved with vehicle (PBS: glycerin = 7: 3,
119 v/v) were applied directly to the wound site once a day.[16, 26] Wound healing was macroscopically
120 monitored by taking digital photographs at the indicated time points with a ruler as reference.
121 Wound areas were calculated from photographs using Image-Pro Plus 6.0 (Adobe Photoshop
122 Element 2.0; Adobe Systems, San Jose, CA, USA; n=12/group). Wound area percentages (% of
123 original wound size) were calculated as the following equation:

124 Wound area (%) at day n = (wound size at day n / wound size at day 0) ×100 %.

125 **Histological Analysis and Immunohistochemistry Analysis on Mice.** 10 × 10 mm biopsy
126 specimens were excised from murine wounds (at days 4 and 14), fixed in 10% paraformaldehyde,
127 and embedded in paraffin wax. Then 5 μm thick sections were prepared and stained with
128 hematoxylin and eosin for histological observations.[27] Image-Pro Plus 6 was used to determine
129 wound changes in five random fields per section. Percentage of re-epithelialization was calculated
130 for 3 sections per wound as the following equation:

131 Re-epithelialization (%) = (distance covered by neoepithelium/distance between wound
132 edges) × 100%

133 For immunofluorescence (IF) staining, 3 μm of paraffin-embedded tissues were stained with
134 anti-F4/80 primary antibody, anti-CD206 primary antibody, anti-α SMA primary antibody, anti-
135 CD31 primary antibody after blocking endogenous peroxidase and nonspecific binding, then with
136 fluorescein-conjugated secondary antibodies.[28] Next they were incubated with biotinylated goat
137 anti-rabbit IgG for 1 h at room temperature. As a control, sections were treated with the same
138 dilution buffer but without primary antibodies. Infiltration of macrophages was evaluated by
139 counting the cells immunostained with anti-F4/80 antibody.

140 **Cell Proliferation Assay.** In order to assess the cytocompatibility of surfactin A with
141 Raw264.7, HaCaT, HDF, and HUVEC cells, MTT assay was performed.[29] Raw 264.7,
142 HaCaT,HDF, and HUVEC cells (10000 cells/well) were separately plated into 96 well plates. After
143 adhering to plates, the cells were incubated for 24 h with vehicle or surfactin A at different
144 concentrations (5, 10, 25, and 50 μg/mL). Then 20 μL MTT solution was added to each well for a
145 further 4 h of incubation at 37 °C. After being washed 3 times with PBS (pH 7.4), the cells were
146 incubated with 160 μL DMSO to dissolve the insoluble formazan product. Absorbance of each
147 well was measured using an ELISA microplate reader at 570 nm. Optical density reflects the level
148 of cells' metabolic activity. Each experiment was performed in quintuplicate.

149 **Scratch Wound-healing Assay.** After starving in medium containing 1% FBS for 24 h,
150 HaCaT, HDF, and HUVEC monolayer cells were given a mechanical scratch wound by a sterile
151 pipette tip. Then floating cells were removed by washing 3 times with PBS.[30] In order to observe
152 the cell migration, cells were treated with vehicle or 25 μg/mL surfactin A in the medium
153 containing 1% FBS. Images of the scratched wound were taken using a microscope immediately
154 and 24 h after wounding. Percentages of the original area size were measured from photographs
155 using Image-Pro Plus 6.0.

156 **ELISA and Western Blot Analysis.** Raw 264.7 cells (1 million cells per well) were seeded
157 to a 6-well culture plate. After 4 h, cells that adhered to the wall were either treated or untreated
158 with 10 μg/mL LPS for 1 h. Vehicle or surfactin A with different concentrations (5, 10, 25, and 50
159 μg/mL) were added to the wells and incubated for another 6 h. Then the cell free supernatants were
160 collected and centrifuged at 10000 g for 10 min. Supernatants obtained were analyzed at the level
161 of IL-6 and TNF-α by a quantitative ELISA using mouse-specific ELISA kit in accordance with
162 the manufacturer's instructions.

163 Expressions of TNF-α, IL-6, HIF-1α, VEGF, TGF-β and α-SMA were detected via western
164 blot assay. For signal pathway studies, HaCaT cells were starved in 1% FBS RPMI for 20 h and
165 then stimulated by 25 μg/mL surfactin A for 15, 30, 60 and 120 min. Samples were collected and
166 lysed in the RIPA lysis buffer with PMSF on ice for 5min. Total protein concentration was
167 determined by BCA assay, followed by separation on a SDS-PAGE gel and electroblotting onto a
168 polyvinylidene fluoride membrane. The membrane was blocked with 5% (w/v) milk in Tris
169 Buffered Saline Tween (TBST), then incubated with primary antibodies at 4 °C overnight. After
170 washing with TBST 4 times, blots were incubated with a secondary antibody for 1 h at room
171 temperature. Blots were washed with TBST 4 times once again, and immunoreactive bands were
172 detected via Gel-Pro-Analyzer (Liuyi, Beijing, China). β-actin was used as an internal indicator.[23]

173 **Statistical Analysis.** All data were analyzed and figured by GraphPad Prism software (version
174 6.0; GraphPad Software, La Jolla, CA). All values are shown as the mean ± SD. Student's t-test
175 was performed to compare the data with paired samples, and two-way ANOVA was applied for
176 multiple group comparisons. For significant interactions, a post hoc multiple comparison test, i.e.,
177 Tukey HSD (honest significant difference) test was performed. P value < 0.05 was considered
178 statistically significant.

179 ■ RESULTS AND DISCUSSION

180 **Identification of the Lipopeptide Fraction with Wound Healing Capability.** In previous
181 study, we have revealed that crude lipopeptides from *B. subtilis* culture exhibited a remarkable
182 promotion of wound healing in a rabbit skin wound model. [26] However, most of the *B. subtilis* can
183 produce at least one type of lipopeptides via fermentation, which always consist of different
184 isoforms and homologous series. Therefore, the fraction of *B. subtilis* crude lipopeptides with

185 wound-healing-promoting property should be further identified. Firstly, crude lipopeptides were
186 separated by C18-RPC column and divided into three major fractions (Frac-1, Frac-2, and Frac-
187 3). After 24 h treatment, Frac-3 significantly promoted wound healing and resulted in minor skin
188 irritation comparing with Frac-1 and Frac-2 (**Figure 1A)**. Next, the Frac-3 was detected by
189 MALDI-TOF-MS to determine its component and molecular mass. Results indicated that Frac-3
190 contained two components (Comp-1 and Comp-2). The Comp-1 was composed of three peaks at
191 m/z of 1022.4705, 1044.4469 and 1060.4192, representing its singly protonated $[M+H]^+$, sodium
192 cationized $[M+Na]^+$, and potassium cationized $[M+K]^+$ adducts, respectively. Whereas three
193 peaks of Comp-2 were measured at m/z values of 1036.4816, 1058.4584 and 1074.4329. Therefore,
194 the observed molecular mass of Comp-1 was 1021.4705 Da and the Comp-2 was 1035.4816 Da
195 (**Figure 1B**). However, only Comp-2 had the activity to promote wound healing (**Figure 1C**).

196 **Figure 1.**

197 The MS/MS spectrum of characteristic ion peaks of Comp-2 were shown in **Figure 2**. MS/MS
198 data of a compound generated a series of *b* and *y* ions that was the main basis for the deduction of
199 amino acid sequences.[31] **Figure 2A** showed the MS/MS spectrum of m/z 1036.4816, and product
200 ions at m/z 1018.8886 $[M-H_2O]^+$ and 923.7941 $[M-Leu]^+$ were observed, which suggested that it
201 was a cyclic surfactin.[32] The specific ion fragments of Comp-2 (Figure 2A) were similar to that of
202 standard surfactin A (Figure 2B).[32] The amino acid sequence of Comp-2 was identified as
203 Glutamic acid^1-Leucine^2-Leucine^3-Valine^4-Asparticacid^5-Leucine^6-Leucine^7 linking to a C15 fatty
204 acid chain, which is consistent with the reported structure of surfactin A[33]. Therefore, standard
205 surfactin A was used to test its potential in the promotion of wound healing.

206 **Figure 2.**

207 **Effects of Surfactin A on Skin Wound Healing *in vivo*.** In order to evaluate the effects of
208 surfactin A on skin wound healing, we performed full-thickness excisional wounds in a murine
209 model. Wound sizes were measured every two days until epithelialization was complete. As shown
210 in **Figure 3A**, surfactin A treatment significantly accelerated the wound healing process as
211 compared with the vehicle-treated group, which had an even better effect than the positive control
212 EGF. Two days after injury, surfactin A- and EGF-treated groups showed a strong wound healing
213 ability than vehicle-treated group. Subsequently, surfactin A-treated murine experienced a rapid
214 acceleration of wound healing in comparison with the vehicle- and EGF-treated group. Until day
215 11, surfactin A-treated wounds were almost completely closed, whereas 15% of the vehicle
216 group's wound areas remained open (**Figure 3B**).

217 **Figure 3.**

218 As surfactin A showed activity to promote wound healing, we undertook further studies to
219 examine the quality of wound healing by histological analysis. Hematoxylin and eosin (H&E)
220 staining revealed that wounds treated with surfactin A showed faster re-epithelialization and
221 smaller granulation tissue compared to murine treated with vehicle throughout the healing process
222 (**Figure 4A**). At day 4, we observed a significant difference in the epidermal thickness of vehicle-
223 and surfactin A-treated groups. At this time, the vehicle-treated group showed little epidermal
224 organization, while significant epidermal regeneration was observed in the surfactin A-treated
225 group (**Figure 4B**). At day 14, the surfactin A- treated group showed a thinner epidermal thickness
226 as compared to the vehicle-treated group. Masson's trichrome staining indicated that granulation
227 tissue was replaced by dense collagen deposition in the surfactin A-treated group, whereas the
228 dermal layer in the other two group was not yet fully regenerated at day 14 (**Figure 4C, D**).

229 The effects of surfactin A on wound healing promotion were extensively studied in view of
230 the whole wound healing process affected by surfactin A application. A murine model with a full-
231 thickness excisional wound demonstrated that surfactin A treatment significantly sped up re-
232 epithelialization compared to vehicle and even EGF treatment. It affected granulation tissue
233 constriction, epithelium thickness and collagen deposition, which are three vital evaluation
234 standards for wound healing. To explain the potential underlying mechanisms for its wound-
235 healing promoting ability, we measured the effects of surfactin A on angiogenesis, cell migration,
236 inflammation, and scar tissue.

237 **Figure 4.**

238 **Effects of Surfactin** A **on Angiogenesis in Wound Tissue.** Angiogenesis, the sprouting
239 of capillaries from pre-existing blood vessels, is essential for the wound healing process. Wound
240 requires a continuous delivery of oxygen and nutrients for sustaining fibroblast proliferation,
241 collagen synthesis, and re-epithelialization.[34] CD31 immumohistochemical staining was
242 conducted to show the new blood vessels formation. At day 4 post wounding, the vehicle-treated
243 wounds had slightly lower blood vessel density compared to the surfactin A-treated wounds
244 (**Figure 5A**), However, the events changed at day 14 post wounding (**Figure 5A**). These results
245 suggested that more efficient wound healing in the wounds treated with surfactin A might result
246 from enhanced angiogenesis in the injured area. At day 14 post wounding, the granulation tissue
247 was mature, the number of capillaries decreased and wound healing was nearly over.

248 As reported, HIF-1α is a very important transcription factor complex and VEGF is a crucial
249 growth factor in revascularization, which have been discovered to play important roles in
250 angiogenesis and wound healing.[35,36] To determine the correlation between the pro-angiogenic
251 effect of surfactin A and the expression of these proteins, we analyzed the possible angiogenic

252 proteins (HIF-1α and VEGF) levels in the wound sites using western blotting. As shown in **Figure**
253 **5,** surfactin A significantly promoted HIF-1α and VEGF protein expression in wounds. Results
254 indicated that surfactin A were able to up-regulate the expression levels of HIF-1α and VEGF to
255 promote angiogenesis and wound healing. Impaired angiogenesis is one of the most common
256 complications in diabetes patients, always resulting in delayed wound healing.[37] In other words,
257 surfactin A may have a role in accelerating the diabetic wound repair and regeneration.

258 **Figure 5.**

259 **Effects of Surfactin** A **on Cell Proliferation and Migration *in vitro*.** Based on the above
260 observation that surfactin A significantly accelerated wound healing in murine, we further
261 explored the effect of surfactin A on cells proliferation involved in the wound healing process *in*
262 *vitro*. **Figure 6A-C** showed surfactin A enhanced the proliferation of HDF cells in a concentration-
263 dependent manner, and a significant proliferation was observed even at 10 μg/mL. However, only
264 a slight effect was found on HaCaT and HUVEC proliferations. During the process of skin wound
265 healing, keratinocytes migrate from the edge of the wound toward the wound bed.[38] Thus the
266 ability of drugs to promote keratinocyte migration is of great significance and we performed
267 scratch assay in the HaCaT, HDF, and HUVEC cells to assess the effect of surfactin A on cell
268 migration. The scratch wound healing assay indicated that surfactin A significantly promoted the
269 migration of HaCaT and HUVEC but only slightly of HDF, as illustrated in **Figure 6D** and **6E**.
270 Migrations of HaCaT and HUVEC across the wound gap were significantly enhanced in surfactin
271 A treated cells as compared with the vehicle treatment. Migration rates reached 79% or 44% after
272 24 h treatment, respectively. These results indicated that surfactin A accelerated wound closure
273 primarily by promoting keratinocytes migration, but not cell proliferation.

274 **Figure 6.**

275 MAPK and NF-κB signaling pathways have been reported to be associated with cell
276 migration.[12] To reveal the molecular mechanism by which surfactin A accelerated cell migration,
277 we assayed the levels of phosphorylated and total protein of ERK, JNK, and p65 by western
278 analysis in HaCaT cells. As shown in **Figure 7**, the p-ERK1/2 are transiently up-regulated between
279 15 min and 30 min after addition of surfactin A, whereas p-JNK are up-regulated after 15 min
280 treatment, then the phosphorylation level gradually decreased. However, surfactin A induced p65
281 up-regulation continued to increase during 120 minutes treatment (**Figure 7**). The ERK1/2
282 phosphorylation level increased by 2.9, 4.4, and 1.9 times after 15, 30, and 60 min surfactin A
283 treatment, the p-JNK phosphorylation level increased by 2.4, 1.8, and 1.8 times, compared with
284 p65 increment in nuclear by 1.6, 2.7, 2.6, and 4.4 times, respectively. Results indicated that
285 surfactin A activated ERK1/2, JNK and NF-κB p65 signaling pathways, thus enhancing the
286 migration of HaCaT cells. Because JNK and NF-κB signaling pathways are reported to involve in
287 TGF-β release and the wound healing process, a cross talk between the pathways regulate TGF-β
288 release and the migration of HaCaT cells warrant further study.[11]

289 **Figure 7.**

290 **Effects of Surfactin A on the Inflammatory Response *in vivo* and *in vitro*.** In the early
291 stage of inflammatory phase, macrophages present a pro-inflammatory phenotype and coordinate
292 wound healing events via phagocytosis of pathogens and cellular debris, as well as by the secretion
293 of growth factors, chemokines, and cytokines, such as TNF-α and IL-6.[39-41] Although a pro-
294 inflammatory environment may contribute to pathogen phagocytosis and death during the early
295 wound healing stage, persistence at the wound site will lead to prolonged wound healing, such as
296 a chronic diabetic wound.[42] In order to identify surfactin A effects on inflammatory response,
297 ELISA and western blot were used to quantify the inflammatory cytokine secretion *in vivo* and *in*

298 *vitro*. As illustrated in **Figure 8A** and **8B**, at day 4 post-injury, surfactin A application reduced
299 IL-6 expression in the murine wounds, while it had little effect on the secretion of TNF-α. In the
300 MTT assay, surfactin A significantly promoted the proliferation of murine macrophage cell (RAW
301 264.7) and significantly inhibited the LPS-induced TNF-α and IL-6 levels in a dose-dependent
302 manner in the culture supernatants of RAW264.7 (**Figure 8A-E**). This indicated that surfactin A
303 could not only promote the recruitment of macrophages, but also inhibit the over-expression of
304 pro-inflammatory cytokines.

305 Macrophages are central players in the wound healing progress which are commonly divided
306 into two phenotypes, classically activated macrophages (M1) and alternatively activated
307 macrophages (M2).[43] M1 macrophages inhibit the formation of blood vessels, whereas M2
308 macrophages promote the formation of blood vessels and produce anti-inflammatory cytokines to
309 suppress the inflammation, which faciliates tissue repair and tissue remodeling. The M1/M2
310 macrophage balance polarization is vital of during the wound healing.[44] As shown in **Figure 8F**,
311 compared to the vehicle group, surfactin A treatment resulted in more macrophages around the
312 wound site and more M2 macrophages appearance (marked by the expression of CD206) than M1
313 macrophages (marked by the expression of F4/80). This indicated that surfactin A promoted the
314 recruit of macrophages to the wound site and the phenotypic switch of M1 to M2 there.

315 Macrophages are vitally necessary for the wound healing process at almost every stage.
316 Macrophages can recruit other macrophages and activate fibroblastic and endothelial cells, all
317 while they produce cytokines to modulate the inflammatory microenvironment. In chronic wound,
318 persistent and excessive inflammation is the main cause of damaged healing.[11] Meanwhile,
319 macrophages phenotypic switch from M1 to M2 at the wound site was found in this work. It is
320 obvious that the regulation of macrophage phenotype is related to tissue microenvironment. When

321 pathogens or infection occur at wound site after injury, macrophages first exhibit the M1
322 phenotype to release pro-inflammatory cytokines such as TNF-α, IL-6 against the stimulus. But
323 continuous M1 macrophages impede wound repair. M2 macrophages secrete high amounts of
324 cytokines such as IL-10 to suppress the inflammation, and contribute to tissue repair, remodeling,
325 vasculogenesis.[43] Therefore, the phenotypic switching of macrophage is very important for
326 wounds to enter the normal repair stage.

327 **Figure 8.**

328 **Effects of Surfactin** A **on Scar Formation.** Hypertrophic scar is a common complication
329 of wound healing. They usually occur after burn injury, trauma and surgery, leading to cosmetic
330 and functional problems.[45] Currently, the widely accepted mechanism of hypertrophic scar
331 formation include excessive production and deposition of extracellular matrix proteins (ECM),
332 prolonged inflammation and other chronic stimuli, and excessive growth of cells.[46] This study
333 showed that surfactin A could inhibit chronic inflammation in the wound and promote cell
334 migration but not cell proliferation (**Figure 6 and Figure 8**). Compared with the control group,
335 fewer granulation tissues, more organized and thinner collagen fibers were formed in the surfactin
336 A-treated wounds (**Figure 4**). In addition, cutaneous appendages, such as hair follicles and sweat
337 glands, also appeared in the surfactin A-treated wounds. These results indicated that surfactin A
338 might be capable to prevent scar formation. Therefore, we further analyzed the effects of surfactin
339 A on scar formation.

340 Wound tissues at day 4 and 14 post wounding were stained with an antibody against α-
341 smooth muscle actin (α-SMA). **Figure 9A** showed strong expression of α-SMA in myofibroblasts
342 of the granulation tissue below the wound at day 4 post wounding in surfactin A-treated murine,
343 but only showed very weak signals in vehicle-treated murine. At day 14 post wounding, expression

344 of α-SMA significantly decreased α-SMA protein expression in wounds, indicating a potential
345 inhibition effect of surfactin A on α-SMA protein expression. TGF-β1 is a key factor to promote
346 transition of fibroblast-to-myofibroblast and formation of extracellular matrix and increase of α-
347 SMA expression.[47] Thus, the expression of TGF-β1 in the wound site were further studied by
348 western blotting. The obtained results showed that surfactin A treatment resulted in a lower TGF-
349 β1 levels than vehicle treatment during the whole healing process. This indicated that surfactin A
350 could down-regulate the expression of TGF-β1 and decrease the expression of α-SMA, and thus
351 reduce the scar formation.

352 TGF-β1 plays a key role in hypertrophic scar formation, which stimulate the transformation
353 of fibroblasts into myofibroblasts.[48] Myofibroblasts are responsible for excessive production and
354 deposition of ECM.[41] TGF-β1 induces quiescent fibroblasts to express α-SMA, a signature protein
355 of myofibroblasts and an important material basis for scar contraction.[49] The obtained results
356 showed that surfactin A might down-regulate the expression of TGF-β1 by TGF-β1/Smad
357 signaling pathway to reduce scar formation.[50]

358 **Figure 9.**

359 Concerns about the pressure of environmental change and resource shortage have provided
360 strong motivations to develop materials with novel functions. Surfactin A from *B. subtilis* was
361 firstly demonstrated to have capability in accelerating the wound healing process via regulating
362 angiogenesis, inflammatory response and cell migration (**Figure 10**). In the livestock industry,
363 wounds caused by falling, beating, smashing, bumping or operation happen so often. Animal
364 wounds are more susceptible to infection by pathogenic microorganisms due to the unclean
365 livestock environment or livestock bodies. Especially in spring, summer and autumn mosquito and

fly bite wounds and aggravate the infection, which slow the healing process leading to a large treatment cost.

Despite promising applications in agriculture and biomedicine, development and prospect of microbial production of surfactin A are limited due to its high costs, low yields and technical constraints on artificial synthesis. To reduce the cost, several waste biomass materials such as corncob hydrolysate, feather hydrolysate waste and glutamate mill waste have been tested as carbon sources for the production of surfactin.[51] Many studies have been conducted to improve the yield of surfactin A by regulating fermentation parameters including pH, temperature, agitation speed, oxygen supply, and medium composition.[52] With the development of genetic engineering and synthetic biology, it is possible to construct high yield, high conversion rate and high production rate strains, and surfactin A might be a cheap, effective and potential alternative drug to promote wound healing in the future. However, further study is still needed to illustrate whether other surfactin fractions from *B. subitlis* also have such capability.

Figure 10.

Funding

This work was supported by the Innovation Foundation for Doctor Dissertation of Northwestern Polytechnical University (Grant No. CX201968), the Modern Agricultural Industry Technology System (CARS-30), the National Natural Science Fund of China (31701722), the Key Research and Development Plan of Shaanxi Province (2017ZDXL-NY-0304, 2019ZDLNY01-02-02), National Key R&D Program of China (2017YFE0105300), the China Postdoctoral Science Foundation (No. 2017M620471), the Shaanxi Provincial Natural Science Foundation (No. 2018JQ3054), and the Postdoctoral Research Project of Shaanxi Province (No. 2017BSHEDZZ103).

389 **Notes**

390 The authors declare that they have no competing interests.

391 ■ **REFERENCES**

392 (1) Cochrane, S. A.; Vederas, J. C. Lipopeptides from *Bacillus* and *Paenibacillus spp.*: A Gold
393 Mine of Antibiotic Candidates. *Med. Res. Rev.* **2016**, 36, 4-31.

394 (2) Ni, H. Y.; Li, N.; Qian, M.; He, J.; Chen, Q.; Huang, Y. H.; Zou, L.; Long, Z. E.; Wang,
395 F. Identification of a Novel Nitroreductase LNR and Its Role in Pendimethalin Catabolism in
396 *Bacillus subtilis* Y3. *J. Agric. Food. Chem.* **2019**, 67, 12816-12823.

397 (3) Olmos, J.; Acosta, M.; Mendoza, G.; Pitones, V. *Bacillus subtilis*, an Ideal Probiotic
398 Bacterium to Shrimp and Fish Aquaculture that Increase Feed Digestibility, Prevent Microbial
399 Diseases, and Avoid Water Pollution. *Arch. Microbiol.* **2020**, 202, 427-435.

400 (4) Mandal, S. M.; Barbosa, A. E. A. D.; Franco, O. L. Lipopeptides in Microbial Infection
401 Control: Scope and Reality for Industry. *Biotechnol. Adv.* **2013**, 31, 338-345.

402 (5) Altenbuchner, J. Editing of the *Bacillus subtilis* Genome by the CRISPR-Cas9 System.
403 *Appl. Environ. Microbiol.* **2016**, 82, 5421-5427.

404 (6) de Araujo, L. V.; Guimaraes, C. R.; Marquita, R. L. D.; Santiago, V. M. J.; de Souza, M.
405 P.; Nitschke, M; Freire, D. M. G. Rhamnolipid and Surfactin: Anti-adhesion/antibiofilm and
406 Antimicrobial Effects. *Food. Control.* **2016**, 63, 171-178.

407 (7) Zhao, H. B.; Xu, X. G.; Lei, S. Z.; Shao, D. Y.; Jiang, C. M.; Shi, J. L.; Zhang, Y. W.; Liu,
408 L.; Lei, S. Z.; Sun, H.; Huang, Q. S. Iturin A-Like Lipopeptides from *Bacillus subtilis* Trigger
409 Apoptosis, Paraptosis, and Autophagy in Caco-2 cells. *J. Cell. Physiol.* **2019**, 234, 6414-6427.

410 (8) Naik, S.; Larsen, S. B.; Gomez, N. C.; Alaverdyan, K.; Sendoel, A.; Yuan, S. P.; Polak,
411 L.; Kulukian, A.; Hai, S. C.; Fuchs, E. Inflammatory Memory Sensitizes Skin Epithelial Stem
412 Cells to Tissue Damage. *Nature.* **2017**, 550, 475-480.

413 (9) Chen, H. L.; Cheng, J. W.; Ran, L. X.; Ran, L. X.; Yu, K.; Lu, B. T.; Lan, G. Q.; Dai, F.
414 Y.; Lu, F. An Injectable Self-Healing Hydrogel with Adhesive and Antibacterial Properties
415 Effectively Promotes Wound Healing. *Carbohyd. Polym.* **2018**, 201, 522-531.

416 (10) Na, J.; Lee, K.; Na, W.; Shin, J. Y.; Lee, M. J.; Yune, T. Y.; Lee, H. K.; Jung, H. S.; Kim,
417 W. S.; Ju, B. G. Histone H3K27 Demethylase JMJD3 in Cooperation with NF-κB Regulates
418 Keratinocyte Wound Healing. *J. Invest. Dermatol.* **2016**, 136, 847-858.

419 (11) Herter, E. K.; Li, D. Q.; Toma, M. A.; Vij, M.; Li, X.; Visscher, D.; Wang, A. X.; Chu,
420 T. B.; Sommar, P.; Blomqvist, L.; Berglund, D.; Stahle, M.; Wikstrom, J. D.; Landen, N. X.
421 WAKMAR2, a Long Noncoding RNA Downregulated in Human Chronic Wounds, Modulates
422 Keratinocyte Motility and Production of Inflammatory Chemokines. *J. Invest. Dermatol.* **2019**,
423 139, 1373-1384

424 (12) Morino-Koga, S.; Uchi, H.; Mitoma, C.; Wu, Z.; Kiyomatsu, M.; Fuyuno, Y.; Nagae,
425 K.; Yasumatsu, M.; Suico, M. A.; Kai, H.; Furue, M. 6-formylindolo[3,2-b] Carbazole Accelerates
426 Skin Wound Healing via Activation of ERK, but Not Aryl Hydrocarbon Receptor. *J. Clin. Invest.*
427 **2017**, 137, 2217-2226.

428 (13) Mandel, H. H.; Sutton, G. A.; Abu, E.; Kelmer, G. Intralesional Application of Medical
429 Grade Honey Improves Healing of Surgically Treated Lacerations in Horses. *Equine. Vet. J.* **2020**,
430 52, 41-45.

431 (14) Adcock, S. J. J.; Vieira, S. K.; Alvarez, L.; Tucker, C. B. Iron and Laterality Effects on
432 Healing of Cautery Disbudding Wounds in Dairy Calves. *J. Dairy. Sci.* **2019**, 102, 10163-10172.

433 (15) Mei, F. F.; Liu, J. J.; Wu, J. T.; Duan, Z. W.; Chen, M. X.; Meng, K. K.; Chen, S. J.;
434 Shen, X. R.; Xia, G. H.; Zhao, M. H. Collagen Peptides Isolated from *Salmo salar* and *Tilapia*
435 *nilotica* Skin Accelerate Wound Healing by Altering Cutaneous Microbiome Colonization via
436 Upregulated NOD2 and BD14. *J. Agric. Food. Chem.* **2020**, 68,1621-1633.

437 (16) Mu, L. X.; Tang, J.; Liu, H.; Shen, C. B.; Rong, M. Q.; Zhang, Z. Y.; Lai, R. A Potential
438 Wound-Healing-Promoting Peptide from Salamander Skin. *Faseb. J.* **2014**, 28, 3919-3929.

439 (17) Chepkirui, C.; Cheng, T.; Sum, W. C.; Matasyoh, J. C.; Decock, C.; Praditya, D. F.;
440 Wittstein, K.; Steinmann, E.; Stadler, M. Skeletocutins A-L: Antibacterial Agents from the Kenyan
441 Wood-Inhabiting Basidiomycete, *Skeletocutis* sp. *J Agric Food Chem*. **2019**, 67, 8468-8475.

442 (18) Wu, Y. B.; Zhou, L. B.; Lu, F. X.; Bie, X. M.; Zhao, H. Z.; Zhang, C.; Lu, Z. X.; Lu, Y.
443 J. Discovery of a Novel Antimicrobial Lipopeptide, Brevibacillin V, from *Brevibacillus*
444 *laterosporus* fmb70 and Its Application on the Preservation of Skim Milk. *J. Agric. Food. Chem.*
445 **2019**, 67, 12452-12460.

446 (19) Zhao, H. B.; Shao, D. Y.; Jiang, C. M.; Shi, J. L.; Li, Q.; Huang, Q. S.; Rajoka, M. S.
447 R.; Yang, H.; Jin, M. L. Biological Activity of Lipopeptides from *Bacillus*. *Appl. Microbiol. Biot.*
448 **2017**, 101, 5951-5960.

449 (20) Chen, W. Y.; Chang, H. Y.; Lu, J. K.; Huang, Y. C.; Harroun, S. G.; Tseng, Y. T.; Li,
450 Y. J.; Huang, C. C.; Chang, H. T. Self-assembly of Antimicrobial Peptides on Gold Nanodots:
451 Against Multidrug-resistant Bacteria and Wound-healing Application. *Adv. Funct. Mater.* ***2015***,
452 25, 7189-7199.

453 (21) Ahire, J. J.; Robertson, D. D.; van, Reenen, A. J.; Dicks, L. M. T. Surfactin-loaded
454 Polyvinyl Alcohol (PVA) Nanofibers Alters Adhesion of *Listeria monocytogenes* to Polystyrene.
455 *Mat. Sci. Eng. C-Mater.* **2017**, 77, 27-33.

456 (22) Zouari, R.; Moalla-Rekik, D.; Sahnoun, Z.; Rebai, T.; Ellouze-Chaabouni, S.; Ghribi-
457 Aydi D. Evaluation of Dermal Wound Healing and *in vitro* Antioxidant Efficiency of *Bacillus*
458 *subtilis* SPB1 Biosurfactant. *Biomed. Pharmacother.* **2016**, 84, 878-891.

459 (23) Zhao, H. B.; Zhao, X. X.; Lei, S. Z.; Zhang, Y. W.; Shao, D. Y.; Jiang, C. M.; Sun,
460 H.; Shi, J. L. Effect of Cell Culture Models on the Evaluation of Anticancer Activity and
461 Mechanism Analysis of the Potential Bioactive Compound, Iturin A, Produced by *Bacillus subtilis*.
462 *Food. Funct.* **2019**, 10, 1478-1489.

463 (24) Lu, Y.; Ye, C.; Che, J. X.; Xu, X. G.; Shao, D. Y.; Jiang, C. M.; Liu, Y. L.; Shi, J. L.
464 Genomic Sequencing, Genome-Scale Metabolic Network Reconstruction, and in Silico Flux
465 Analysis of the Grape Endophytic Fungus *Alternaria* sp. MG1. *Microb. Cell. Fact.* **2019**, 18, 13.

466 (25) Cerqueira, M. T.; Pirraco, R. P.; Santos, T. C.; Rodrigues, D. B.; Frias, A. M.; Martins,
467 A. R.; Reis, R. L.; Marques, A. P. Human Adipose Stem Cells Cell Sheet Constructs Impact
468 Epidermal Morphogenesis in Full-thickness Excisional Wounds. *Biomacromolecules.* **2013**, 14,
469 3997-4008.

470 (26) Yan, L.; Liu, G. W.; Wang, X. L.; Jiang, C. M.; Shao, D. Y.; Shi, J. L. Identification and
471 Characterization of Lipopeptides as a Potential Wound Healing Agent Produced by *Bacillus*
472 *subtilis. BIBE 2019, The Third International Conference on Biological Information and*
473 *Biomedical Engineering*, Hangzhou, China, **2019**, 1-4.

474 (27) Huang, Y. W.; Zhu, Q. Q.; Yang, X. Y.; Xu, H. H.; Sun, B.; Wang, X. J.; Sheng, J. Wound
475 Healing can be Iimproved by (-)-epigallocatechin Gallate through Targeting Notch in
476 Streptozotocin-Induced Diabetic murine. *Faseb. J.* **2019**, 33, 953-964.

477 (28) He, R. G.; Yin, H.; Yuan, B. H.; Liu, T.; Luo, L.; Huang, P.; Dai, L. C.; Zeng, K. IL-33
478 Improves Wound Healing through Enhanced M2 Macrophage Polarization in Diabetic murine.
479 *Mol. Immunol.* **2017**, 90, 42-49.

480 (29) Vergaro, V.; Abdullayev, E.; Lvov, Y. M.; Zeitoun, A.; Cingolani, R.; Rinaldi, R.;
481 Leporatti, S. Cytocompatibility and Uptake of Halloysite Clay Nanotubes. *Biomacromolecules.*
482 **2010**, 11, 820-826.

483 (30) Hu, Y.; Rao, S. S.; Wang, Z. X.; Cao, J.; Tan, Y. J.; Luo, J.; Li, H. M.; Zhang, W. S.;
484 Chen, C. Y.; Xie, H. Exosomes from Human Umbilical Cord Blood Accelerate Cutaneous Wound
485 Healing through miR-21-3p-mediated Promotion of Angiogenesis and Fibroblast Function.
486 *Theranostics.* **2018**, 8, 169-184.

487 (31) Ma, Z. W.; Hu, J. C. Production and Characterization of Surfactin-type Lipopeptides as
488 Bioemulsifiers Produced by a Pinctada Martensii-derived *Bacillus mojavensis* B0621A. *Appl.*
489 *Biochem. Biotech.* **2015**, 177, 1520-1529.

490 (32) Tang, J. S.; Zhao, F.; Gao, H.; Dai, Y.; Yao, Z. H.; Hong, K.; Li, J.; Ye, W. C.; Yao, X.
491 S. Characterization and Online Detection of Surfactin Isomers Based on HPLC-MS^n Analyses and
492 Their Inhibitory Effects on the Overproduction of Nitric Oxide and the Release of TNF-alpha and
493 IL-6 in LPS-Induced Macrophages. *Mar. Drugs*. **2010**, 8, 2605-2618.

494 (33) Aleti, G.; Lehner, S.; Bacher, M.; Compant, S.; Nikolic, B.; Plesko, M.; Schuhmacher,
495 R.; Sessitsch, A.; Brader, G. Surfactin Variants Mediate Species-specific Biofilm Formation and
496 Root Colonization in *Bacillus*. *Environ. Microbiol.* **2016**, 18, 2634-2645.

497 (34) Kant, V.; Gopal, A.; Kumar, D.; Pathak, N. N.; Ram, M.; Jangir, B. L.; Tandan, S. K.;
498 Kumar, D. Curcumin-induced Angiogenesis Hastens Wound Healing in Diabetic Rats. *J. Surg.*
499 *Res.* **2015**, 193, 978-988.

500 (35) Wu, Y. S.; Ngai, S. C.; Goh, B. H.; Chan, K. G.; Lee, L. H.; Chuah, L. H. Anticancer
501 Activities of Surfactin and Potential Application of Nanotechnology Assisted Surfactin Delivery.
502 *Front. Pharmacol.* **2017**, 8, 761.

503 (36) Kong, L. Z.; Wu, Z.; Zhao, H. K.; Cui, H. M.; Shen, J.; Chang, J.; Li, H. Y.; He, Y. H.
504 Bioactive Injectable Hydrogels Containing Desferrioxamine and Bioglass for Diabetic Wound
505 Healing. *Appl Mater. Interfaces.* **2018**, 10, 30103-30114.

506 (37) Kota, S. K.; Meher, L. K.; Jammula, S.; Kota, S. K.; Krishna, S. V.; Modi, K. D. Aberrant
507 Angiogenesis: The Gateway to Diabetic Complications. *Indian. J. Endocrinol. Metab.* **2012**, 16,
508 918-930.

509 (38) Zhu, Q.; Mangukiya, H. B.; Mashausi, D. S.; Guo, H.; Negi, H.; Merugu, S. B.; Wu, Z.;
510 Li, D. Anterior Gradient 2 is Induced in Cutaneous Wound and Promotes Wound Healing through
511 its Adhesion Domain. *FEBS. J.* **2017**, 284, 2856-2869.

512 (39) Tymen, S. D.; Rojas, I. G.; Zhou, X.; Fang, Z. J.; Zhao, Y.; Marucha, P. T. Restraint
513 Stress Alters Neutrophil and Macrophage Phenotypes during Wound Healing. *Brain. Behav.*
514 *Immun*. **2013**, 28, 207-217.

515 (40) Wang, J.; Kubes, P. A Reservoir of Mature Cavity Macrophages that can Rapidly Invade
516 Visceral Organs to Affect Tissue Repair. *Cell.* **2016**, 165, 668-678.

517 (41) Jiang, Z. W.; Liu, Y. Q.; Li, C. W.; Chang, L. L.; Wang, W.; Wang, Z. H.; Gao, X. G.;
518 Ryffel, B.; Wu, Y. L.; Lai Y. P. IL-36gamma Induced by the TLR3-SLUG-VDR Axis Promotes
519 Wound Healing via REG3A. *J. Invest. Dermatol.* **2017**, 137, 2620-2629.

520 (42) Kim, S. Y.; Nair, M. G. Macrophages in Wound Healing: Activation and Plasticity.
521 *Immunol. Cell. Biol.* **2019**, 97, 258-267.

522 (43) Moghaddam, A.; Mohammadian, S.; Vazini, H.; Taghadosi, M.; Esmaeili, S. A.; Mardani,
523 F.; Seifi, B.; Mohammadi, A.; Afshari, J. T.; Sahebkar, A. Macrophage Plasticity, Polarization and
524 Function in Health and Disease. *J. Cell. Physiol.* **2018**, 233, 6425-6440.

525 (44) Mnif, I.; Grau-Campistany, A.; Coronel-Leon, J.; Hammami, I.;, Triki, M. A.; Manresa,
526 A.; Ghribi, D. Purification and Identification of *Bacillus subtilis* SPB1 Lipopeptide Biosurfactant
527 Wxhibiting Antifungal Activity Against R*hizoctonia bataticola* and *Rhizoctonia solani*. *Environ.*
528 *Sci. Pollut. Res.* **2016**, 23, 6690-6699.

529 (45) Bai, X. Z.; Liu, J. Q.; Yang, L. L.; Fan, L.; He, T.; Su, L. L.; Shi, J. H.; Tang, C. W.;
530 Zheng, Z.; Hu, D. H. Identification of Sirtuin 1 as a Promising Therapeutic Target for Hypertrophic
531 Scars. *Brit. J. Pharmacol.* **2016**, 173, 1589-1601.

532 (46) Tyack, Z.; Simons, M.; Spinks, A.; Wasiak, J. A Systematic Review of the Quality of
533 Burn Scar Rating Scales for Clinical and Research Use. *Burns* **2012**, 38, 6-18.

534 (47) Werner, S.; Grose, R. Regulation of Wound Healing by Growth Factors and Cytokines.
535 *Physiol. Rev.* **2003**, 83, 835-870.

536 (48) Gabbiani, G. The Myofibroblast in Wound Healing and Fibrocontractive Diseases. *J.*
537 *Pathol.* **2003**, 200, 500-503.

538 (49) Hoerst, K.; van den Broek, L.; Sachse, C.; Klein, O.; von Fritschen, U.; Gibbs, S.;
539 Hedtrich, S. Regenerative Potential of Adipocytes in Hypertrophic Scars is Mediated by
540 Myofibroblast Reprogramming. *J. Mol. Med.* **2019**, 97,761-775.

541 (50) Sarrazy, V.; Billet, F.; Micallef, L.; Coulomb, B.; Desmoulière, A. Mechanisms of
542 Pathological Scarring: Role of Myofibroblasts and Current Developments. *Wound. Repair. Regen.*
543 **2011**, 19, 10–15.

544 (51) Chen, C.; Lin, J. Z.; Wang, W. D.; Huang, H.; Li, S. Cost-Effective Production of
545 Surfactin from Xylose-Rich Corncob Hydrolysate Using *Bacillus subtilis* BS-37. *Waste. Biomass.*
546 *Valori.* **2019**, 4, 341-347.

547 (52) Yi, G. B.; Liu, Q.; Lin, J. Z.; Wang, W. D.; Huang, H.; Li, S. Repeated Batch
548 Fermentation for Surfactin Production with Immobilized *Bacillus subtilis* BS-37: Two-Stage pH
549 Control and Foam Fractionation. *J. Chem. Technol. Biot.* **2017**. 92. 520-525

550

551 **TOC graphic**

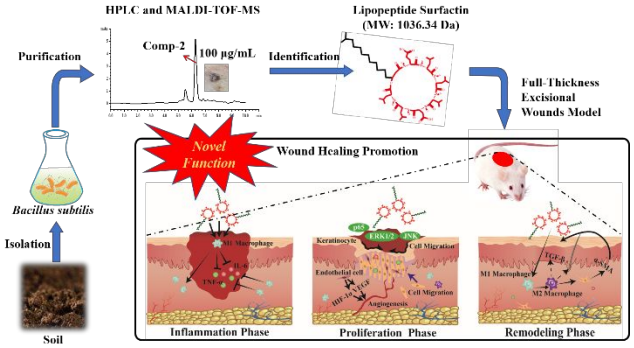

552

553 **Figure Captions**

554 **Figure 1.** RPC and HPLC chromatograms at analysis of the wound-healing-promoting fraction
555 from *B. subtilis*. (A) RPC Chromatogram of crude lipopeptides from *B. subtilis*, Frac-3 was
556 identified as the major fraction to promote wound healing. (B) MALDI-TOF-MS spectra of Frac-
557 3 which contained two components with m/z at 1021.4705 (Comp-1) and 1035.4816 (Comp-2).
558 (C) HPLC Chromatogram of Frac-3, Comp-2 (MW: 1035.4816) was the active fraction of *B.*
559 *subtilis* crude lipopeptides to promote wound healing.

560 **Figure 2.** MS/MS spectrum and chemical structures of the Comp-2. (A) Fragmentations of Comp-
561 2 by tandem MS to generate b and y ions. (B) The fragmentations of surfactin standard. The b and
562 y ions of surfactin (B) were corresponding that of Comp-2 (A) at the values of gaps less than 0.5
563 m/z. Comp-2 is a cyclic surfactin A containing a Glutamicacid^{1}-Leucine^{2}-Leucine^{3}-Valine^{4}-
564 Asparticacid^{5}-Leucine^{6}- Leucine^{7} peptide precursor (C) and C15 fatty acid chains (D).

565 **Figure 3.** Effects of surfactin A on skin wound healing *in vivo*. (A) Vehicle (PBS: glycerin = 7:3,
566 v/v), Surf (100 μg/mL), or EGF (100 μg/mL) was applied to 7 mm full-thickness excisional
567 wounds made on the backs of Kunming murine once a day. Images of a representative mouse from
568 each group taken post-injury on days1, 4, 7, 11, and 14. White rulers beneath wound served as
569 reference. (B) Wound area percentages (% original wound size) on different days post-injury were
570 determined by analyzing the wound closure in photos (n = 6). * indicated significant differences
571 between control, surfactin A, and EGF groups; # indicated significant differences between Surf
572 and EGF group, $P < 0.05$.

573 **Figure 4.** H&E and Massion staining. (A) Images of skin wounds stained with H&E on days 4, 7,
574 and 14. Vertical dashed lines indicated the wound edge and arrows indicated the ends of migrating

575 epithelial cells. Scale bar, 500 μm. (B) Re-epithelialization rates and epidermal thickness were
576 measured (n = 6). (C) Images of skin wounds stained with Mason's Trichrome on days 4, 7, and
577 14. Scale bar, 500 μm. (D) Areas of collagen deposition (blue areas) were measured (n = 6). *P <
578 0.05.

579 **Figure 5.** Effects of surfactin A on angiogenesis in the wound tissue. (A) Histological analysis of
580 CD31 expression in wound tissue at day 4 and day 14 postwounding (n = 6). The black arrows
581 indicated the new blood vessels. (B) Levels of HIF-1α and VEGF determined by western analysis
582 from samples of excised wound tissues from murine at day 4 and day 14 post-wounding with or
583 without surfactin A treatment. (C) and (D) Relative density of HIF-1α and VEGF secretions in
584 skin wounds (n = 6). Pixel density was expressed as a ratio to β-actin and normalized to vehicle
585 treated murine. A statistically significant difference is indicated by an asterisk (*P < 0.05; **P <
586 0.01).

587 **Figure 6.** Effects of surfactin A on the proliferation, migration, and invasion of HaCaT, HDF, and
588 HUVEC cells. (A) HaCaT, (B) HDF, (C) HUVEC cell proliferations were measured after 24 h
589 treatments with vehicle or surfactin A with indicated concentrations by MTT assay (n = 5). (D)
590 Scratch wound healing assay of HaCaT, HDF, and HUVEC cells treated with vehicle or surfactin
591 A 25 μg/mL. Black dotted line demarcated original scratch edges and red dotted line demarcated
592 the ends of migrating cells. Scale bar was 50 μm. E) Percentages of the original area were measured
593 (n = 4). *P < 0.05.

594 **Figure 7.** Effects of surfactin A on MAPK and NF-κB signaling pathways in HaCaT cells. (A),
595 (B), and (C) Effects of surfactin A (25 μg/mL) on ERK and JNK protein kinases phosphorylation
596 and the time-course. (D) and (E) Effects of surfactin A (25 μg/mL) on p65 translocation in nuclear
597 proteins and the time-course. The densitometry of phosphorylated ERK and JNK were normalized

598 to total ERK and JNK (n = 6). A statistically significant difference is indicated by an asterisk (*P
599 < 0.05; **P < 0.01).

600 **Figure 8.** Effects of surfactin A on inflammatory cytokine secretion *in vivo* and *in vitro*. (A)
601 Western blot of TNF-α and IL-6 secretions in skin wounds on day 4 post-injury. (B) Relative
602 density of TNF-α and IL-6 secretions in skin wounds (n = 6). (C) RAW 264.7 cell proliferations
603 were measured after 24 h treatment with either vehicle or surfactin A with indicated concentrations
604 by MTT assay (n = 5). Effects of (D) TNF-α and (E) IL-6 secretions in RAW 264.7 cells induced
605 by LPS were measured after 6 h treatment with vehicle or surfactin A with indicated
606 concentrations. *P < 0.05. (F) Effects of surfactin A on macrophage polarization at day 14 post-
607 wounding. Wound section was stained with the macrophage marker F4/80 (green) and the M2
608 marker CD206 (red). The white arrows indicated the M2-type macrophages.

609 **Figure 9.** Effects of surfactin A on scar formation in the wound tissue. (A) Histological analysis
610 of α-SMA expression in wound tissue at day 4 and day 14 postwounding (n = 6). The black arrows
611 indicated the positive cell. (B) Levels of TGF-β1 determined by western analysis from samples of
612 excised wound tissues from murine at day 4 and day 14 post-wounding with or without surfactin
613 A treatment. (C) Relative density of TGF-β1 secretions in skin wounds (n = 6). Pixel density was
614 expressed as a ratio to β-actin and normalized to vehicle treated murine. A statistically significant
615 difference is indicated by an asterisk (*P < 0.05; **P < 0.01).

616 **Figure 10.** Schematic diagram of surfactin A promoting healing in a full-thickness excisional
617 wound model.

618

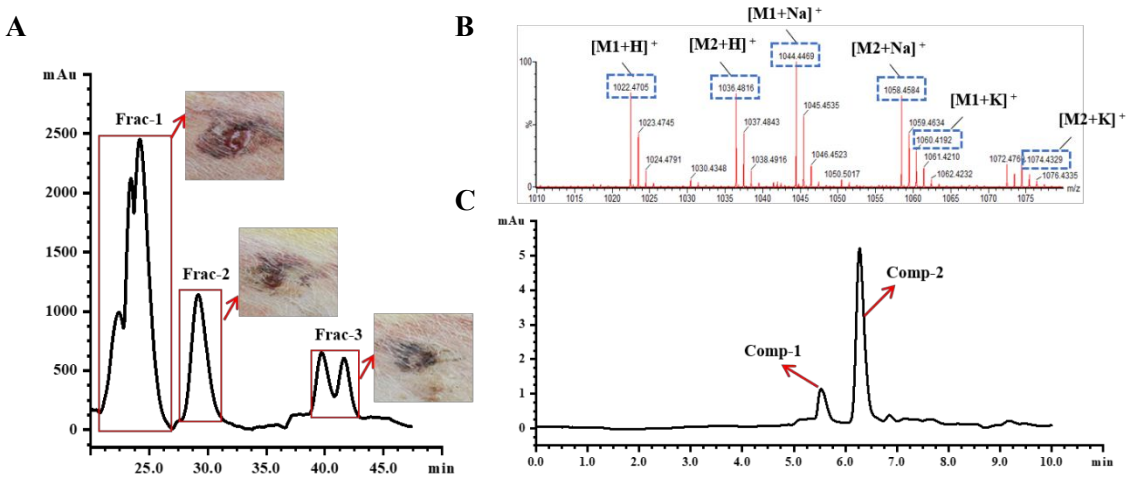

619 **Figure 1**

620

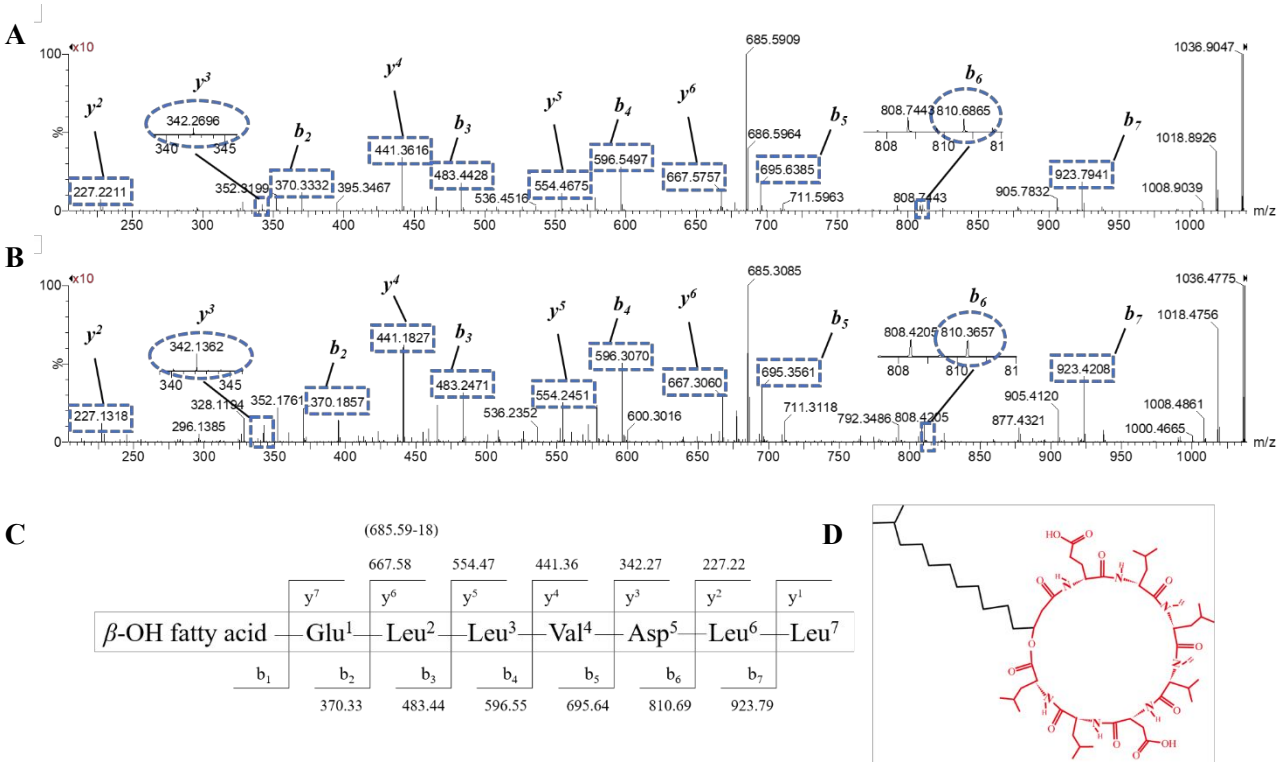
A
B
C
D
(685.59-18)
667.58
554.47
441.36
342.27
227.22
β-OH fatty acid — Glu1 — Leu2 — Leu3 — Val4 — Asp5 — Leu6 — Leu7
370.33
483.44
596.55
695.64
810.69
923.79

621 **Figure 2**

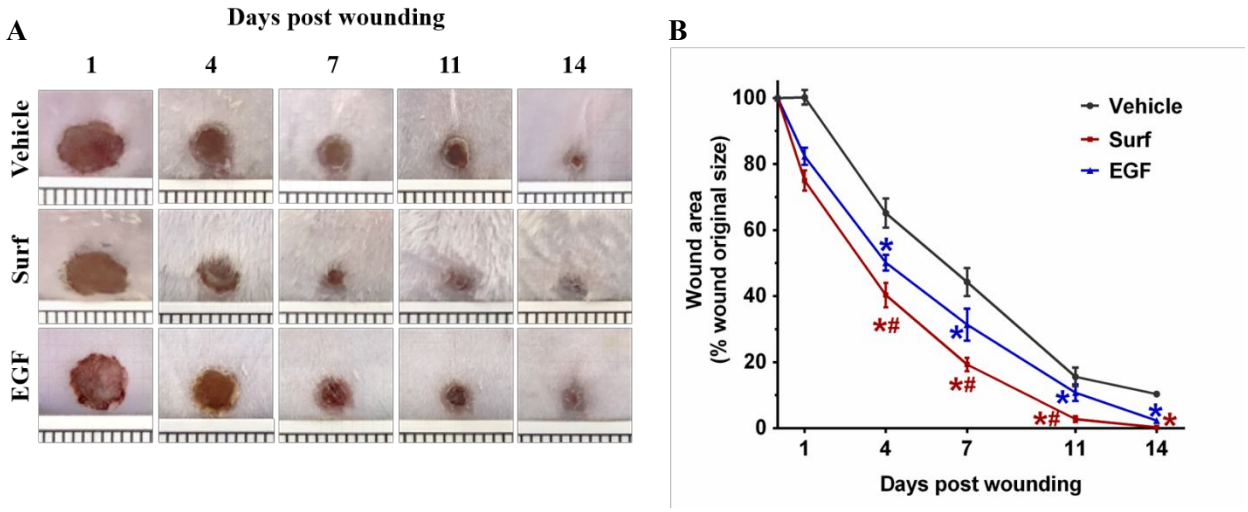
A
Days post wounding
1
4
7
11
14
Vehicle
Surf
EGF
B
Vehicle
Surf
EGF
Wound area
(% wound original size)
100
80
60
40
20
0
1
4
7
11
14
Days post wounding

622 **Figure 3.**

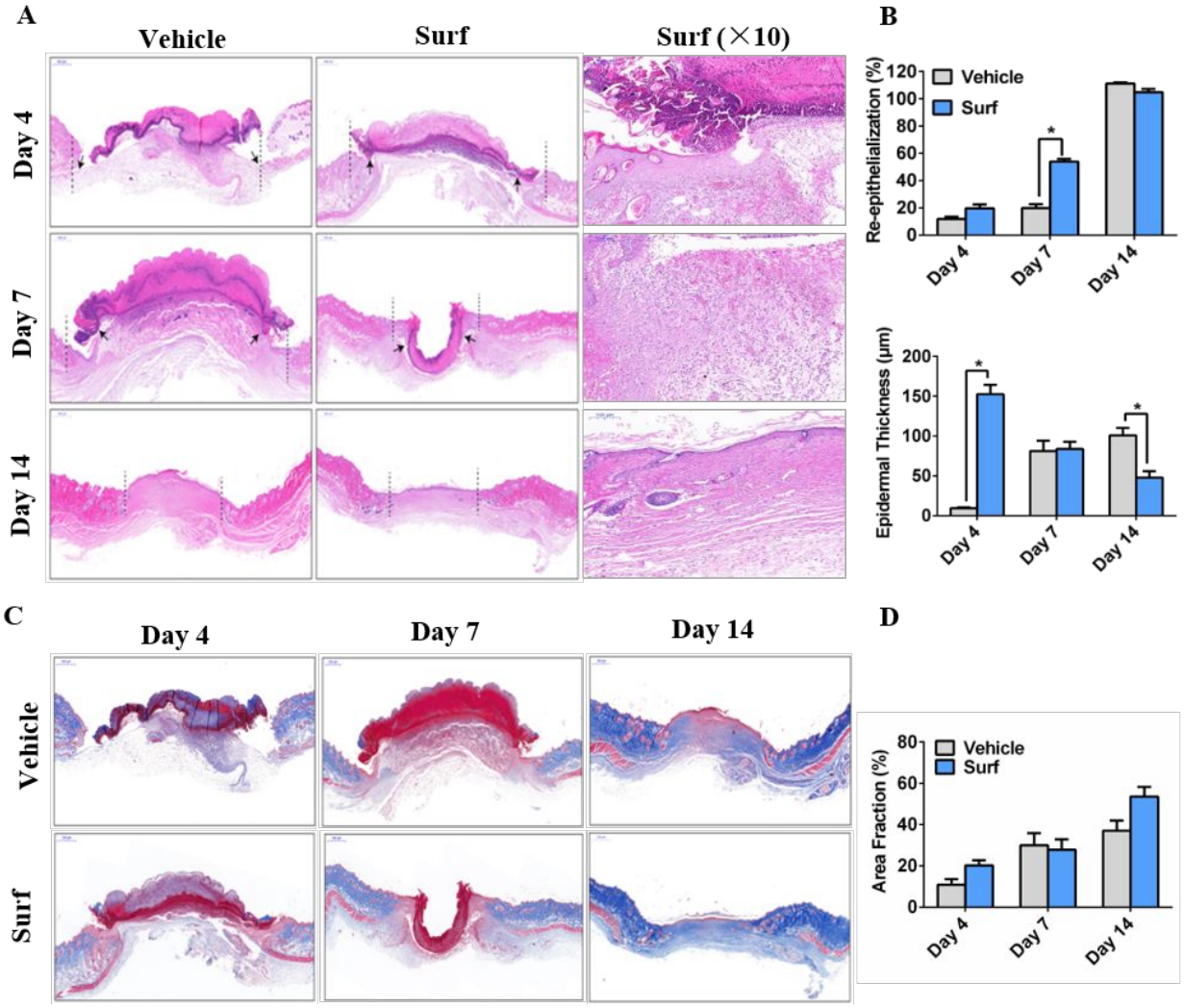
A
Vehicle
Surf
Surf (×10)
Day 4
Day 7
Day 14
B
Re-epithelialization (%)
Vehicle
Surf
Day 4
Day 7
Day 14
Epidermal Thickness (μm)
C
Day 4
Day 7
Day 14
Vehicle
Surf
D
Area Fraction (%)
Vehicle
Surf

623 **Figure 4.**

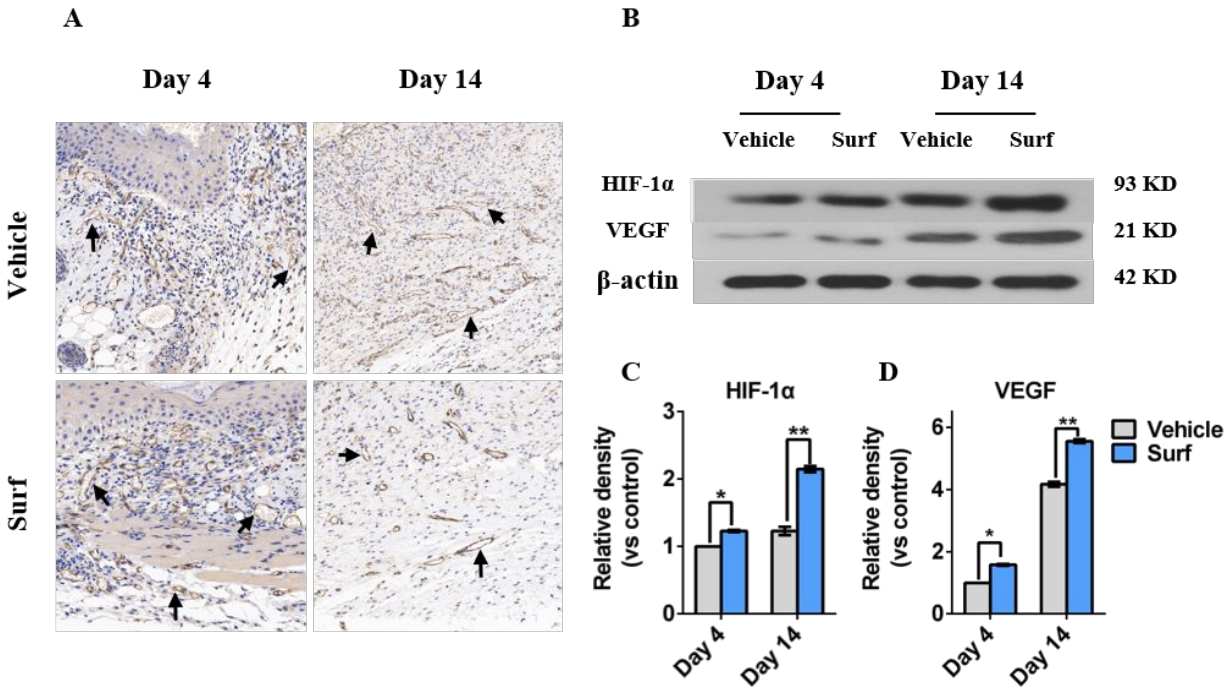
A
Day 4
Day 14
Vehicle
Surf
B
Day 4
Day 14
Vehicle
Surf
Vehicle
Surf
HIF-1α
VEGF
β-actin
93 KD
21 KD
42 KD
C
HIF-1α
Relative density (vs control)
Day 4
Day 14
D
VEGF
Relative density (vs control)
Day 4
Day 14
Vehicle
Surf

624 **Figure 5.**

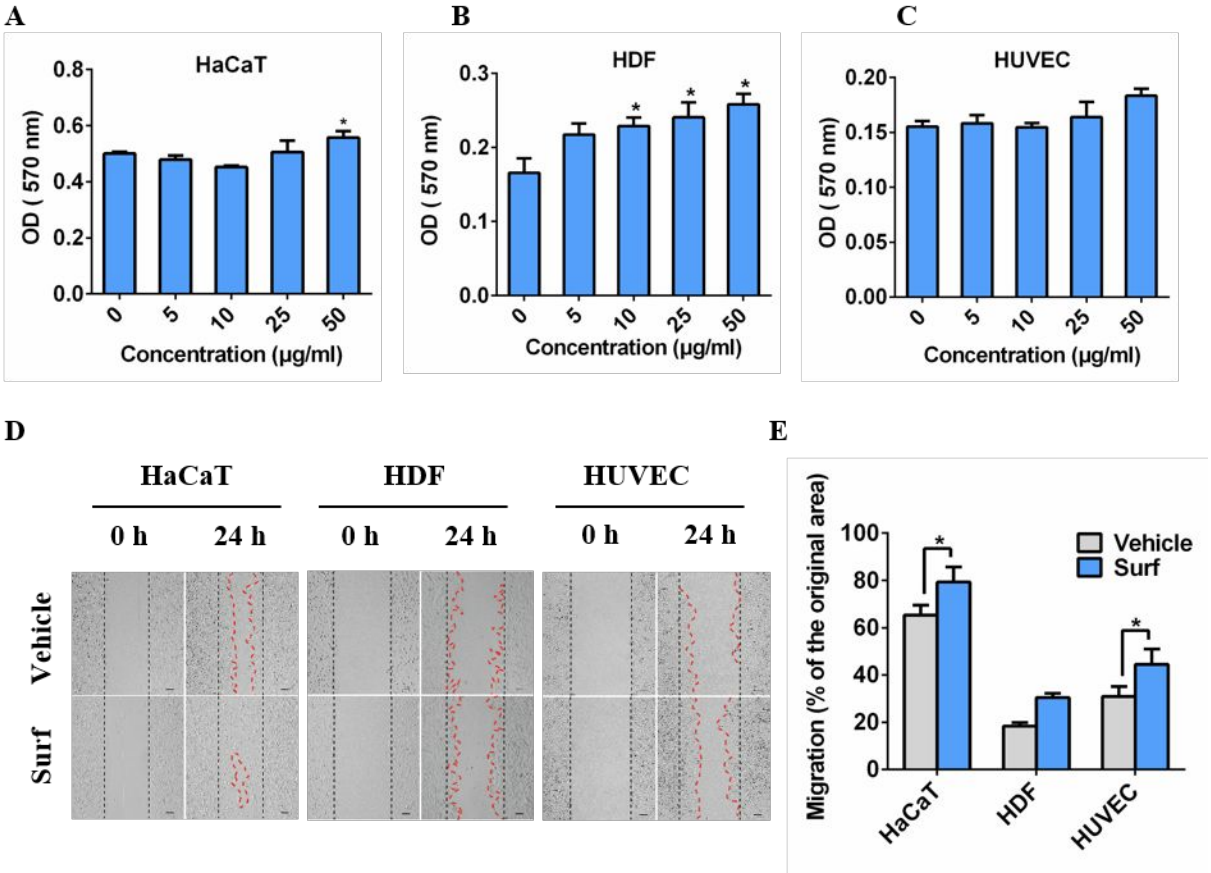
A
HaCaT
OD (570 nm)
0.8
0.6
0.4
0.2
0.0
0
5
10
25
50
Concentration (μg/ml)
B
HDF
OD (570 nm)
0.3
0.2
0.1
0.0
Concentration (μg/ml)
C
HUVEC
OD (570 nm)
0.20
0.15
0.10
0.05
0.00
Concentration (μg/ml)
D
HaCaT
HDF
HUVEC
0 h
24 h
Vehicle
Surf
E
Migration (% of the original area)
100
80
60
40
20
0
Vehicle
Surf
HaCaT
HDF
HUVEC

625 **Figure 6.**

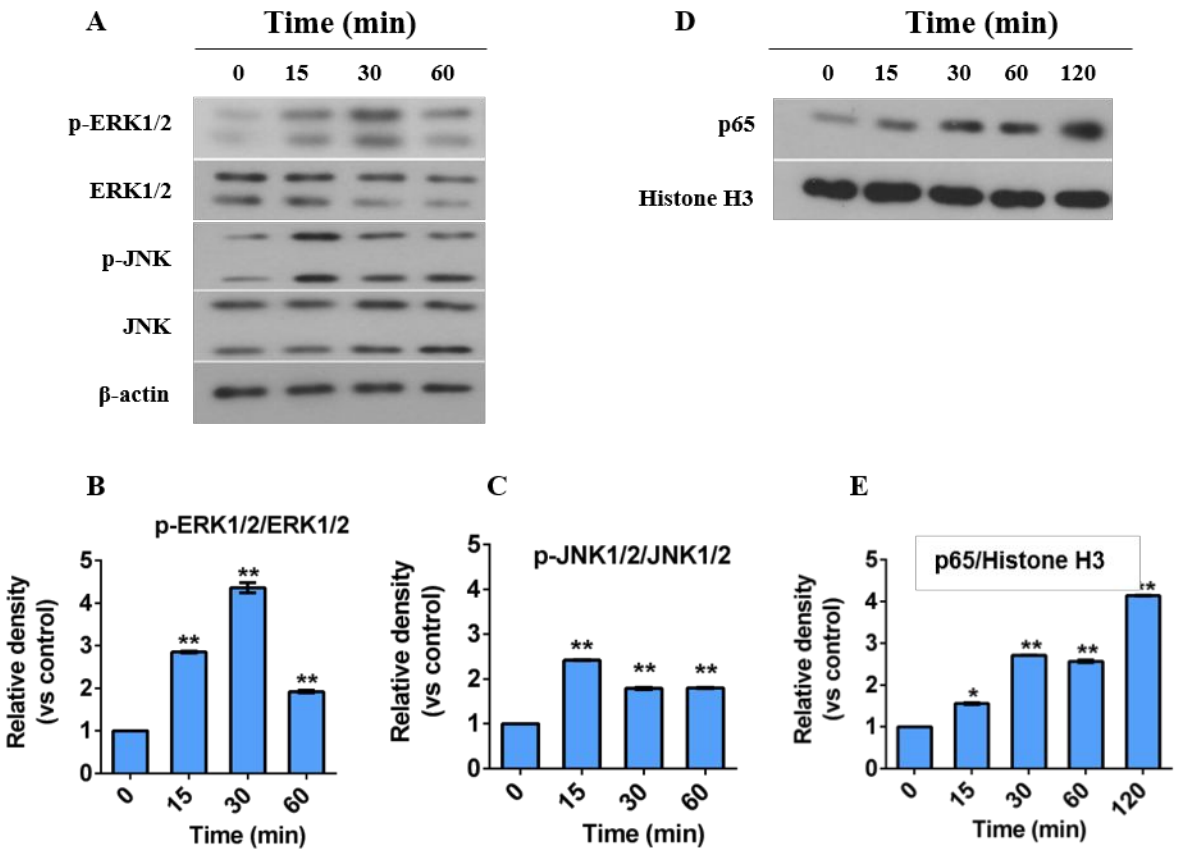

626

627 **Figure 7.**

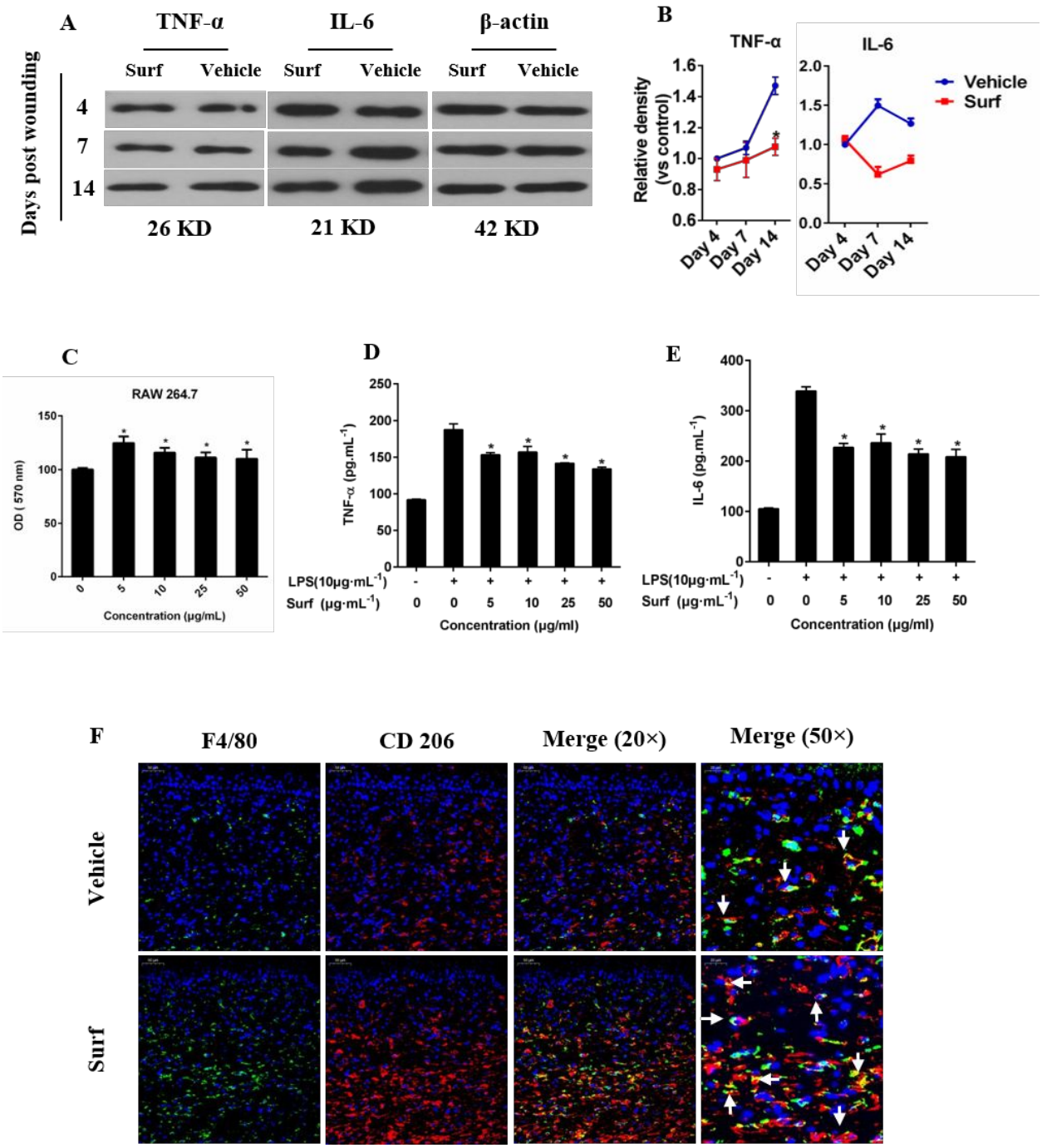
A
TNF-α
IL-6
β-actin
Surf
Vehicle
Days post wounding
4
7
14
26 KD
21 KD
42 KD
B
TNF-α
IL-6
Relative density (vs control)
Vehicle
Surf
Day 4
Day 7
Day 14
C
RAW 264.7
OD (570 nm)
Concentration (μg/mL)
D
TNF-α (pg.mL-1)
LPS(10μg·mL-1)
Surf (μg·mL-1)
Concentration (μg/ml)
E
IL-6 (pg.mL-1)
LPS(10μg·mL-1)
Surf (μg·mL-1)
Concentration (μg/ml)
F
F4/80
CD 206
Merge (20×)
Merge (50×)
Vehicle
Surf

Figure 8.

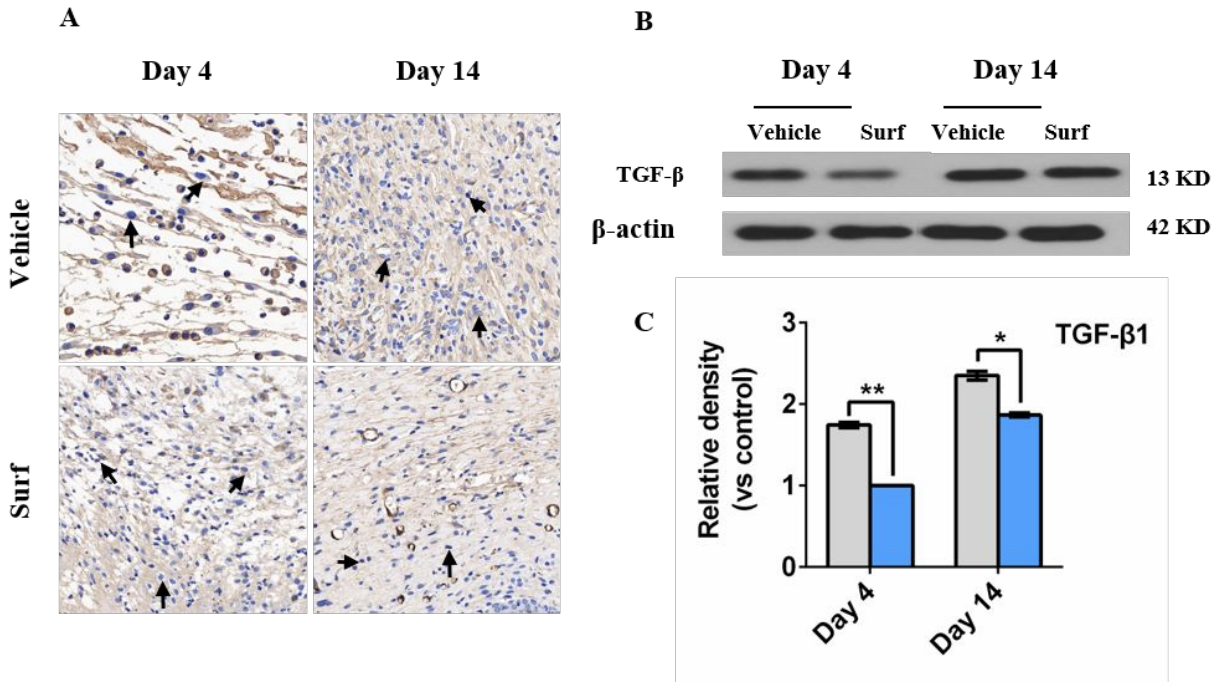

630

631 **Figure 9.**

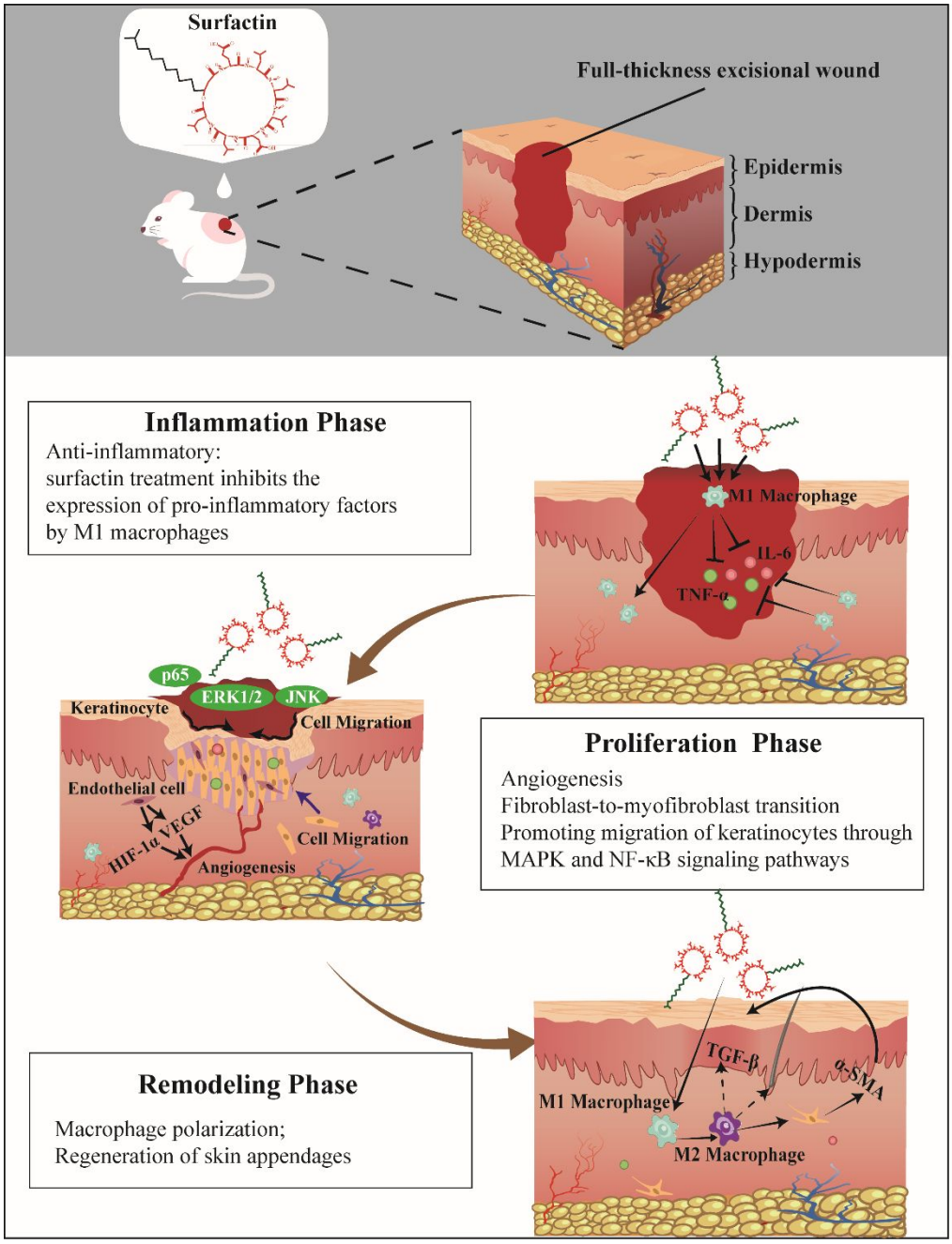

632 **Figure 10.**

633